RSC Applied Polymers

ROYAL SOCIETY OF CHEMISTRY

PAPER

View Article Online
View Journal | View Issue

Cite this: *RSC Appl. Polym.*, 2025, **3**, 361

Healing filler–matrix interfaces in drawn BN/UHMWPE composites by a simple thermal annealing treatment†

Xiangyan Yu,[a,d] Qichen Zhou,[d] Xiaoxiao Yu,[b,c] Man Zhang,[e] Coskun Kocabas,[b,c] Han Zhang,[a] Dimitrios G. Papageorgiou,[a] Haixue Yan,[a] Michael John Reece[a] and Emiliano Bilotti*[d,a]

Received 28th November 2024,
Accepted 20th January 2025

DOI: 10.1039/d4lp00349g

rsc.li/rscapplpolym

Thermally conductive polymer dielectrics have great potential in modern electronic systems by efficiently dissipating the generated heat and thus decreasing the working temperature. Here, unfunctionalised boron nitride microplatelets (BN) and macromolecular alignment, induced by solid-state drawing, were adopted to increase the thermal conductivity of ultra-high-molecular-weight-polyethylene (UHMWPE). A thermal annealing treatment was then utilised to heal filler–matrix interface defects, created during drawing, to enhance the dielectric properties. In particular, an annealed UHMWPE/1 wt% BN composite film with a draw ratio of 20 showed a 20% increase in breakdown strength and a slight increase in charge–discharge efficiency to 94%. This finding demonstrates a simple and fast method to optimize the dielectric and thermal conduction properties of polymer composites films, without the need of any filler surface functionalisation, which promises widening applicability of polymer film capacitors.

1. Introduction

Polymer dielectrics play a very important role in electronics such as capacitors and electronic packaging. However, their low thermal conductivity largely limits the heat dissipation and thus unavoidably results in heat build-up and limited temperature ratings. Meanwhile, heat dissipation is becoming an ever more important issue along with the development of miniaturised, high-power and high-speed electronic systems. So far, a variety of thermally conductive fillers have been incorporated into polymers to improve their thermal conductivity and thus heat dissipation efficiency. Promising values have been achieved only at very high filler concentrations, while sacrificing other properties like mechanical and, more importantly, dielectric properties.[1,2] One of the underlying causes for such a compromise in properties lies in the poor filler–matrix interfaces. To tackle this problem, one strategy is the surface modification of the fillers, to improve their compatibility with the polymer matrix.[3–11] However, the surface modifications, in most cases, involves complicated synthesis and characterisation steps, as well as low yields. Here, we incorporated unfunctionalized hexagonal boron nitride (BN) microplates into UHMWPE, followed by uniaxial solid-state drawing to achieve high macromolecular orientation and hence high thermal conductivity. BN has very good electrically insulative property. It has been reported that the single crystal hexagonal boron nitride has a breakdown strength as high as 1200 MV m^{-1} when the external field is in the direction of its *c*-axis,[12] comparable to diamond (~1000 MV m^{-1}).[13] Besides, it also has a high thermal conductivity, ~400 W m^{-1} K^{-1}.[14,15] UHMWPE has a great potential on achieving high thermal conductivity after molecular alignment by uniaxially stretching, with values up to 104 W m^{-1} K^{-1} for a draw ratio of 400.[16] Unfortunately, solid-state drawing can also introduce defects, including voids and debonding of the filler/matrix interface. Herein, a simple thermal annealing treatment was employed to partially heal such defects, resulting in an increase in breakdown strength and a decrease in dielectric loss.

2. Experimental methods

2.1. Materials

Elinova® material grade, a multi-layer platelet-like hexagonal Boron Nitride powder (BN), was purchased from Thomas Swan. Ultra-high-molecular-weight-polyethylene (UHMWPE) was obtained from Royal DSM in the Netherlands (Stamylan

[a]*School of Engineering and Materials Science, Queen Mary University of London, London, E1 4NS, UK*
[b]*Department of Materials, University of Manchester, Manchester, M13 9PL, UK*
[c]*National Graphene Institute, University of Manchester, Manchester, M13 9PL, UK*
[d]*Department of Aeronautics, Imperial College London, SW7 2AZ, UK. E-mail: e.bilotti@imperial.ac.uk*
[e]*School of Mechanical Engineering, University of Leeds, Woodhouse lane, Leeds, LS2 9JT, UK*

†Electronic supplementary information (ESI) available. See DOI: https://doi.org/10.1039/d4lp00349g

UH 034), with a weight-average molecular mass of approximately 3.3×10^6 g mol^{-1} and an average particle size (D50) of 150 μm. Xylene was purchased from Thermo Fisher Scientific Inc. (The Netherlands).

2.2. Sample preparation

Pure UHMWPE and BN/UHMWPE composite films were prepared through a two-step process involving solution casting and solid-state drawing. To prepare the films, BN (at 1 and 7.5 wt% concentrations) were dispersed in xylene using ultrasonication at full power and room temperature for approximately 1 hour until visible aggregates disappeared. UHMWPE powder was then added to the dispersion, followed by a second ultrasonication step at room temperature for 30 minutes after degassing. The mixture was continuously stirred in an oil bath at around 125 °C until the Weissenberg effect (a phenomenon observed in viscoelastic fluids[17]) became evident. Subsequently, the mixture was kept at 125 °C without stirring for 2 hours to fully dissolve the UHMWPE in xylene, resulting in UHMWPE solutions with a concentration of 1 wt%. These solutions were cast into aluminium trays and air cooled to room temperature. After 7 days of evaporation at room temperature, dry films were obtained. The same procedure was followed to fabricate pure UHMWPE films, excluding the dispersion and introduction of fillers. The resulting films were then cut into rectangular specimens measuring 22 mm × 48 mm. These specimens underwent a two-stage solid-state drawing process to achieve specific draw ratios (DR, defined as the ratio of the final length to the initial length). The first stage of drawing, up to a DR of 20, was performed at 120 °C, while the second stage was conducted at 125 °C. The drawing process was carried out using a universal tensile tester (Instron 5900R84, U.K.) equipped with an environmental chamber, with a crosshead speed of 320 mm min^{-1}. To determine the draw ratio, ink marks were made on the surface of the specimen at regular intervals of 2 mm prior to the drawing process, and the displacement of these marks was measured. The specimens were labelled as B-*x*-DR-*y*, while the pure UHMWPE specimen was labelled as PURE-DR-*y*. In these labels, *x* denotes the content of boron nitride (in wt%) and *y* represents the draw ratio. Table S1† gives a summary of the fabricated BN/UHMWPE samples.

Thermal annealing is carried out by putting the drawn samples (without constraint) into a furnace (Thermo Electron LED GmbH) preheated at 100 °C for 20 min. After the heat treatment, the samples were taken out from the oven and cooled by air.

2.3. Characterization

Scanning electron microscopy (SEM) (FEI Phenom, the Netherlands) analysis was carried out on the BN filler and the surface of the drawn pure UHMWPE and BN/UHMWPE composite films. Raman spectroscopy was performed on a Renishaw inVia Raman Microscope using a 442 nm laser. The scans were performed with a 50 s accumulation time and shift range of 3000–900 cm^{-1}. Transmission electron microscopy (TEM) was conducted with a JEM-F200 field emission transmission electron microscope. Optical Microscopy (OPM) was carried using an Olympus BX60 microscope, in transmitted light mode. *In situ* high temperature OPM was implemented by mounting a Linkam stage (HFS600), on the specimen stage of the optical microscope, and heating the films at a speed of 1 °C min^{-1} until melting. The Linkam stage enabled the modulation of the temperature and heating speed of the sample.

The thermal conductivity (K) was determined using the equation below:

$$K = C_H \cdot \rho \cdot \alpha \quad (1)$$

In this equation, C_H represents the heat capacity (under constant pressure) of the samples, 1.8 J kg^{-1} K^{-1} for UHMWPE and 794.4 J kg^{-1} K^{-1} for BN, ρ stands for the density, taken approximately as 1000 kg m^{-3} for UHMWPE and 210 kg m^{-3} for BN, and α represents the thermal diffusivity in m^2 s^{-1}. C_H and ρ of BN/UHMWPE composites was calculated by the direct rule of mixtures. To measure the thermal diffusivity (α), a custom-built setup was utilized. This setup consisted of a pulsed tunable laser beam (superK COMPACT supercontinuum) with a frequency of 1 Hz, which generated heat waves that propagated periodically into the sample. An infrared camera with high resolution (FLIR T660) was used as a detector. The camera was equipped with an IR micro-lens with a pixel size of 50 × 50. The thermal diffusivity was determined using the Angstrom method. For each sample (30 mm × 10 mm), 10 measurements were conducted along the direction parallel to the solid-state drawing direction.[18,19]

Gold electrodes, with a thickness of approximately 100 nm and a diameter of either 2 mm (for bipolar hysteresis loop measurements) or 5 mm (for dielectric spectroscopy measurements), were sputtered onto both sides of the drawn films. Bipolar hysteresis loops were obtained at room temperature using a ferroelectric tester (NPL, Teddington, UK) with a triangle waveform and a frequency of 10 Hz.[20,21] It should be noted that the maximum voltage generated by the tester was 10 kV, limiting the field that could be applied to relatively thick specimens. The frequency dependence of the dielectric properties was characterized using a Precision Impedance Analyser (4294A, Agilent, Santa Clara, CA).

The charge–discharge efficiency (η) is determined by the ratio of the electric energy discharged relative to the electric energy charged, which is ascertained through the analysis of the displacement–electric field (D–E) loops. The term $(1 - \eta)$ can be construed as the measure of energy loss, commonly referred to as dielectric loss. The two-parameter Weibull analysis equation was utilised to determine the breakdown strength (E_b) of the drawn UHMWPE and UHMWPE/BN nanocomposites during ferroelectric hysteresis tests:[22,23]

$$P(E) = 1 - \exp\left[-\left(\frac{E}{E_b}\right)\right]^{\beta} \quad (2)$$

For each film sample, a minimum of ten specimens were subjected to testing to obtain the experimental breakdown

field (E). The statistical cumulative probability of dielectric breakdown ($P(E)$) and the Weibull parameter (β), were also considered in the analysis.

3. Results and discussion

3.1. Drawn pure UHMWPE and BN/UHMWPE composites films

The SEM and TEM images reveal that the BN fillers have an average size of 1 micro-meter (Fig. 1a–c), with a hexagonal crystalline structure, verified by the diffraction pattern in Fig. 1c. Even though dispersed by ultra-sonication for a long time in diluted isopropanol solution, the BN platelets have a tendency to form aggregates with a dimension of several micro-meters (Fig. 1a). The Fig. 1d–l show the optical microscopy of pure drawn UHMWPE and BN/UHMWPE composites. Pure drawn UHMWPE with different draw ratios all show an obviously fibrous morphology. At a draw ratio of 20, there are nearly no obvious defect within the ordered and fibrous area. Further drawing from 20 to 60 draw ratio led to a more fibrous morphology but also generated more defects (appeared as black dots and denoted by the red cycles). The drawn composite films also showed a highly oriented and fibrous morphology. Since the BN is not transparent and has a lateral dimension ~1 μm, it scattered visible light and appeared as small black dots in the optical microscopic images. From Fig. 1g–i, it can be observed that 1 wt% BN was distributed relatively uniformly in the UHMWPE matrix, with only a slight aggregation evident in low draw ratio samples (λ = 20). However, when the filler content was increased to 7.5 wt%, serious filler aggregation was observed in composite films, at all draw ratios, appearing as clusters of black lines composed of BN aggregates (Fig. 1j–l). Independently from the filler distribution, the introduction of BN induced transverse cracks (perpendicular to the drawing direction) in the films, for draw ratios of 40 or higher (pointed by black arrows). Transverse cracks are associated to the deteriorated drawability and preliminary over-drawing, possibly caused by poor compatibility and thus poor interface between BN and UHMWPE matrix.

In addition to the optical microscopic results, the SEM images (Fig. 2) of the surface of the drawn pure UHMWPE and BN/composites films all showed fibrous morphology, with higher draw ratios imparting a more oriented and fibrous morphology. The BN filler is observable on the surface of the composites with high draw ratio, *e.g.* B1-DR60 and B7.5-DR60. In B7.5-DR60, large voids parallel to the drawing direction are formed, some of which are larger than 20 μm, causing a

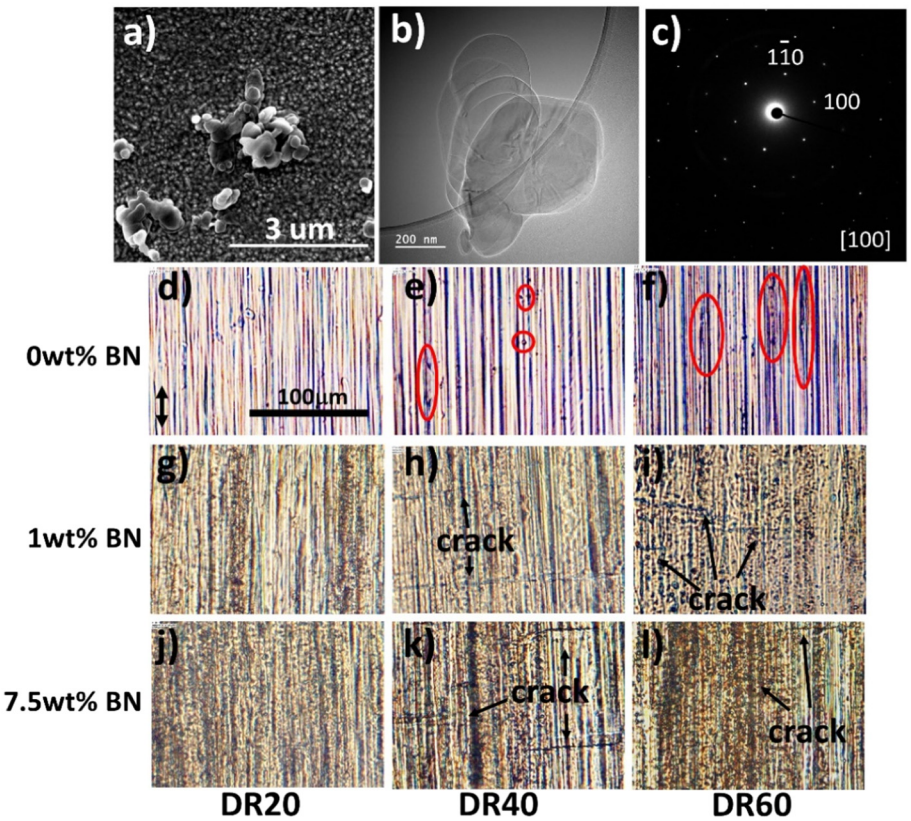

Fig. 1 (a) SEM micrograph. (b) TEM micrograph. (c) Diffraction pattern of BN filler, indexed by PDF#85-1068. (d–l) Optical microscopic images of drawn pure-UHMWPE and BN/UHMWPE composites with different filler concentrations and draw ratios (from the left to the right: films with draw ratio of 20, 40 and 60; from top to the bottom: films with 0, 1, 7.5 wt% BN fillers; double arrows denote the drawing direction).

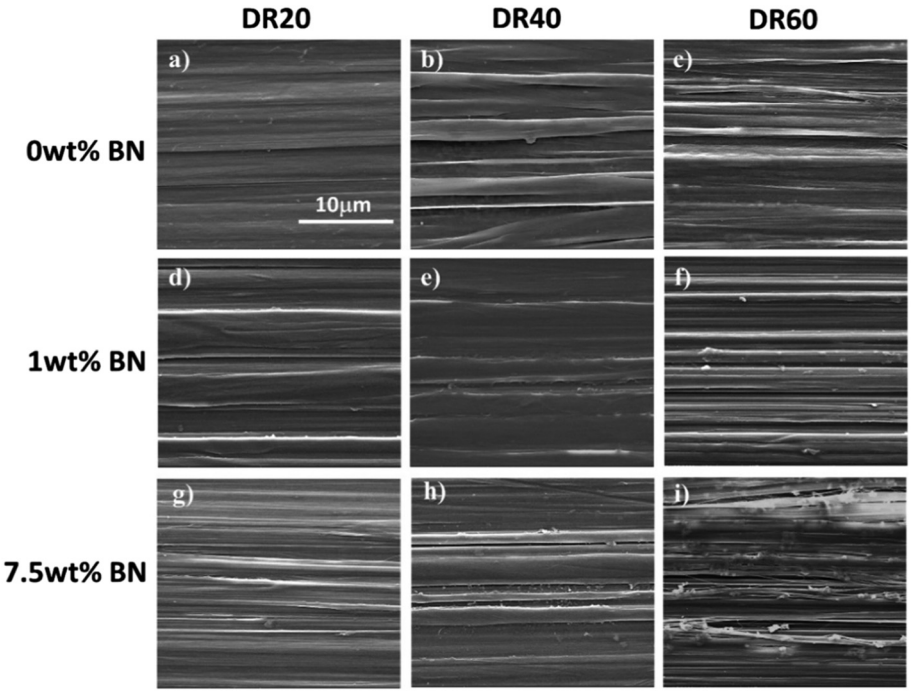

Fig. 2 SEM images of the lateral surface of pure UHMWPE and BN/UHMWPE composites films with different draw ratios. (a) PURE-DR20, (b) PURE-DR40, (c) PURE-DR60, (d) B1-DR20, (e) B1-DR40, (f) B1-DR60, (g) B7.5-DR20, (h) B7.5-DR40, (i) B7.5-DR60.

partial fibrillation of the film. Some of BN agglomerates, located closer to the external surface of the films, seem to have been detached from the polymer matrix and migrated to the external surface during drawing.

Fig. 3 shows the Raman spectroscopy of the drawn films. Peaks at 1129 and 1062 cm^{-1} represent in-phase and out-of-phase all-*trans* C–C stretching vibrations, which come from the orthorhombic crystalline phase and extended chains in the amorphous phase produced by the uniaxial drawing. The sharp peak at 1365 cm^{-1} is the characteristic peak of BN and is due to the E_{2g} phonon mode, which is analogous to the G peak in graphene.[24,25] For the drawn BN/UHMWPE composites, the intensity of the 1365 cm^{-1} peak increased along with the BN content. The area between 1200 and 1500 cm^{-1} of PURE-DR20, B1-DR20 and B7.5-DR20 is enlarged for clarity in the insets (Fig. 3). The peak at 1295 and 1415 cm^{-1} in all three samples are related to CH_2-twisting vibration and CH_2-bending vibration in crystal phase, respectively.[26]

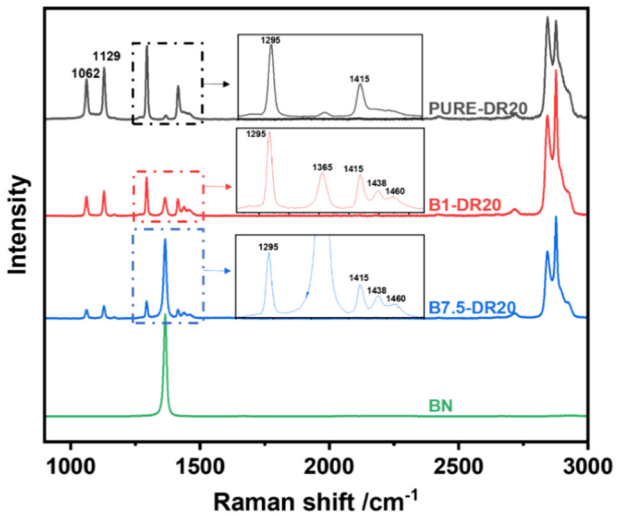

Fig. 3 Raman spectroscopy of the drawn UHMWPE and BN/UHMWPE composite films: PURE-DR20, B1-DR20, B7.5-DR20 and the filler BN. The inset figure shows the enlarged spectroscopy between 1200 and 1500 cm^{-1}.

The main difference of the Raman spectroscopy between the pure matrix and composites with draw ratio of 20 lies in the two peaks 1438 and 1460 cm^{-1} which relate to the amorphous phase of UHMWPE. The occurrence of the peak at 1438 cm^{-1} can be attributed to a random coil structure characterised by multiple gauche bonds, while the peak at 1460 cm^{-1} corresponds to the presence of chain assemblies primarily in the *trans* conformation, but lacking the organised arrangement typically found in the crystalline phase. In the pure matrix with draw ratio of 20, the two peaks are quite broad and hardly recognizable. In the composites with the same draw ratio, the two peaks at 1438 and 1460 cm^{-1} become very obvious, verifying higher amorphous phase content induced by the introduction of BN.[27]

The breakdown strength (E_b) of the drawn films are shown in Fig. 4a and b. Increasing the draw ratio from 20 to 60 slightly decreased the breakdown strength of pure polymer films, possibly because of the voids and defects generated by the drawing process. At all three draw ratios, 1 wt% BN gave

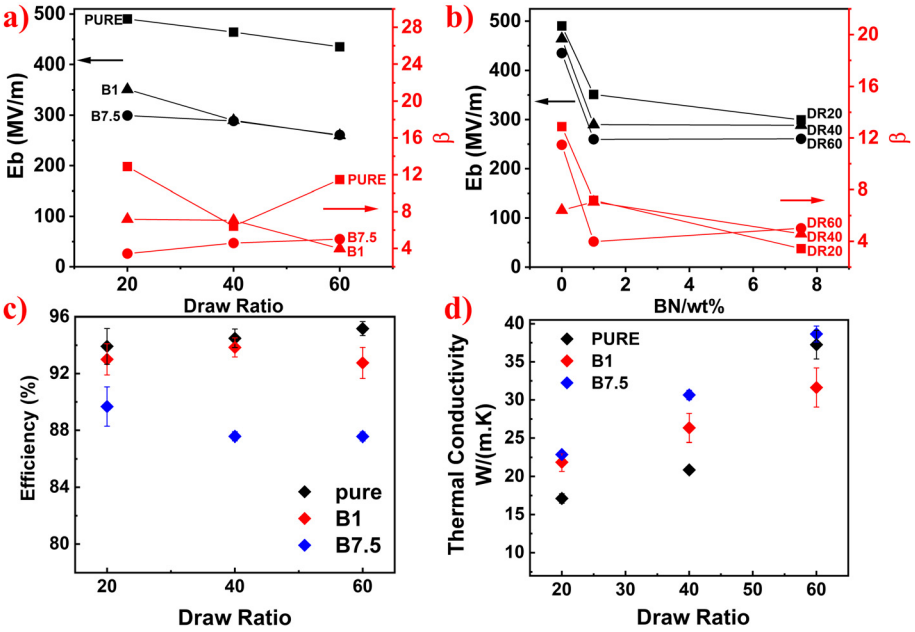

Fig. 4 (a–b) Breakdown strength of the drawn pure UHMPWE and BN/UHMWPE composites films as a function of the filler content and draw ratio, respectively. (c) Charge–discharge efficiency of the drawn pure UHMPWE and BN/UHMWPE composites with 0, 1, 7.5 wt% BN, at 20, 40, 60 draw ratios and 100 MV m^{-1}. (d) The thermal conductivity of drawn pure UHMPWE and BN/UHMWPE composites.

rise to a large drop of the breakdown strength, more than 100 MV m^{-1}. A further increase in filler content to 7.5 wt%, however, did not bring about significant other changes in breakdown strength. This behaviour can be explained by the different levels of filler dispersion in BN/UHMWPE composites with different BN content and of breakdown strength of the phases. Weak interfaces and defects are introduced with the addition of BN in the UHMWPE matrix, causing premature breakdown, under high electric field, which explains the large drop of E_b by 1 wt% BN. However, increasing the BN content from 1 to 7.5 wt% induced a significant filler agglomeration (lower level of filler dispersion), which might have limited the expected increase of surface area with filler content, partially compensated by the beneficial effect of the intrinsic high breakdown strength of BN.

As for the charge–discharge efficiency (η), shown in Fig. 4c, an introduction of 1 wt% BN did not have a significant influence on the charge–discharge efficiency of samples with draw ratios of 20/40. However, higher filler loading resulted in much higher decrease, for all draw ratios. Addition of 7.5 wt% BN led to a decrease of 3.5% for film with draw ratio of 20 and 8% for films with draw ratio of 40 and 60. The poor filler–matrix interface and the filler agglomeration deteriorated the drawability of composite films and caused a large increase in defects and voids upon drawing, when compared to pure polymer films, which therefore increased the dielectric loss, particularly at higher draw ratios. Correspondingly, the dielectric spectroscopy results (Fig. S1†) also reveal the increased tan δ along with the increase content of BN.

Though the breakdown strength and charge–discharge efficiency were decreased a bit, the thermal conductivity can be increased significantly (Fig. 4d). At a high draw ratio of 60, the increase of thermal conductivity is negligible. This can be explained by the large volume of voids near the polymer/filler interface, created by overdrawing, which is detrimental to the heat transfer efficiency. On the contrary, at draw ratio of 20 and 40, the positive effect of the highly thermally conductive BN fillers surpassed the negative effect of the deteriorated interface and increased void content, the introduction of BN largely increased the thermal conductivity of UHMWPE.

3.2. Effect of thermal annealing

The introduction of BN filler led to an enhancement of thermal conductivity of UHMWPE, but it caused an increase of dielectric loss and a decrease of breakdown strength because of the weak interface between BN and UHMWPE matrix. The interface was deteriorated during the drawing process, generating more defects and thus resulting in a larger decrease of charge–discharge efficiency by BN, particularly at higher draw ratios. A thermal annealing treatment (100 °C for 20 min) was attempted to partially heal the defects generated during the drawing process.

After the thermal annealing treatment, the breakdown strength of B1-DR20, B7.5-DR20 and B1-DR40 largely increased by 20%, 27% and 19%, respectively, but that of B7.5-DR60 decreased by 43% (Fig. 5). For other samples (*i.e.* PURE-DR20/40/60, B1-DR60, B7.5-DR40/60), the anneal treatment had a neglectable effect on the breakdown strength (Fig. S2†). The detailed values of the breakdown strength are presented in Table S2.† One assumption for this phenomenon is that the thermal annealing treatment could improve the filler–matrix interfaces by partially healing the small voids generated by the

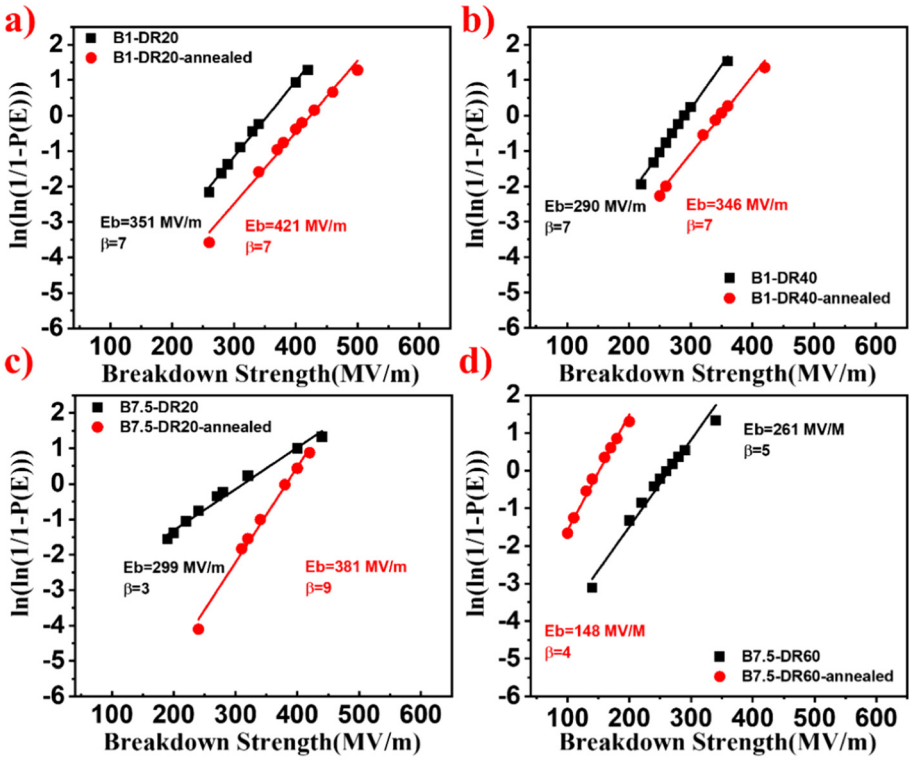

Fig. 5 Weibull distribution of the breakdown strength of and (a) B1-DR20, (b) B1-DR40, (c) B7.5-DR20 and (d) B7.5-DR60, before and after the thermal annealing treatment.

introduction of BN fillers, while enlarging the large voids (*e.g.* transverse cracks) in composite films with large draw ratio (*i.e.*, 60).

However, more evidence would be needed to confirm this hypothesis.

As for the dielectric spectroscopy, the thermal annealing treatment had only minor effects, with dielectric constant being unchanged (Fig. 6a). The charge–discharge efficiency, on the other hand, increased for both 1 wt% and 7.5 wt% BN/UHMWPE composites at low draw ratios of 20 or 40 (Fig. 6c and d), while slightly decreased for pure UHMWPE, at all three draw ratios (Fig. 6b), and largely decreased for composites with the largest draw ratio of 60 (Fig. 6c and d).

In Fig. S3,† it can be observed that the thermal annealing treatment decreased the thermal conductivity for all the samples with different filler concentrations and draw ratios. The effect of thermal annealing is partially analogous to the effect of lowering the draw ratio, as the entropy of the polymer macromolecules increases (*i.e.* orientation decreases) upon relaxation.[28] However, the annealing treatment did not change the overall dimensions of the films. Therefore, it could have affected the morphology at a microscopic level, without influencing their macroscopic characteristics, which could be potentially used to tailor and refine the thermal and dielectric properties to meet specific requirements.

To further explore the related mechanism, *in situ* optical microscopy was used to study the morphology change of the B7.5-DR60 (Fig. 7a–d) at elevated temperature. The fibrous morphology, originated from the drawn UHMWPE matrix, was preserved up to a temperature of 142 °C. The white straight lines are the transverse cracks perpendicular to the drawing direction, caused by overdrawing (draw ratio = 60). During thermal annealing, there is no observable change on the crack when heated to 140 °C. However, when the temperature reached 142 °C (very near to the melting temperature of 145 °C, Fig. S5†), the crystal cluster, composed of highly oriented molecules on either side of the crack, started to contract, verified by the enlarged crack and more curved crystal clusters. Further increasing the temperature to 144 °C not only enlarged the crack more seriously but also gave rise to a partial melting (*i.e.* a structural collapse from the top of the observed area), caused by the uneven heating process.

To interpret the increased breakdown strength by anneal treatment for composite films with low draw ratio and the decreased breakdown strength for films with both high filler content and draw ratio, the following mechanism can be formulated. During the mild anneal treatment (100 °C for 20 minutes), molecular relaxation was accelerated, reducing the orientation of extended chains and increasing self-diffusion. As a result, small defects (especially longitudinal voids) could be healed or partially healed to smaller sizes (leading to increased charge–discharge efficiency for samples in relatively good quality, Fig. 6c and d), unlike large transverse voids and cracks, which could even be enlarged (Fig. 7a–d). However, the breakdown strength of the drawn pure matrix, at any draw ratios, did not change after this anneal treatment

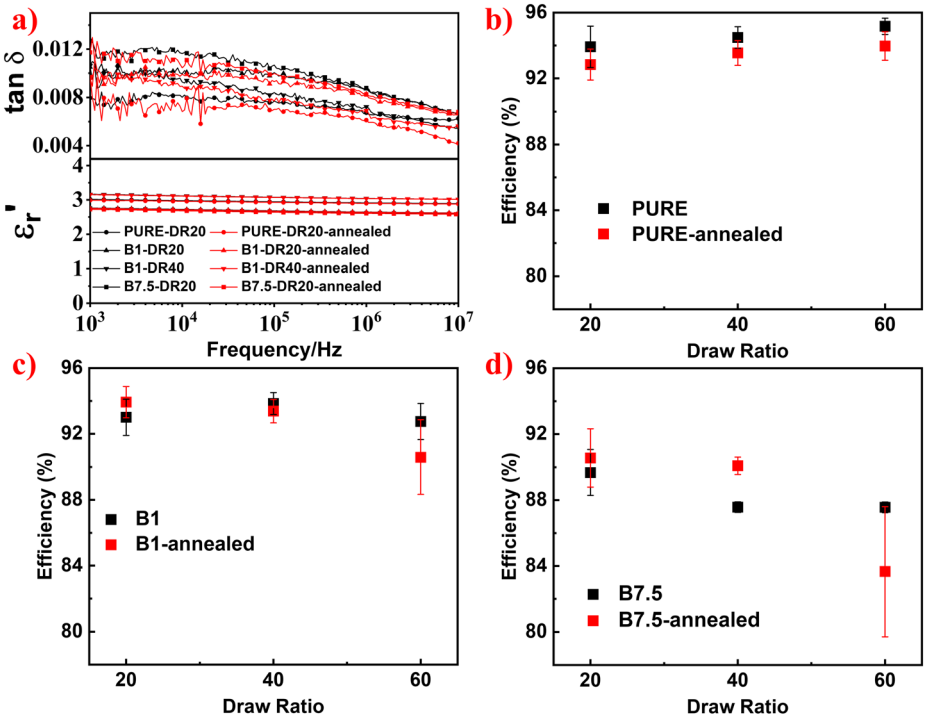

Fig. 6 (a) The dielectric constant and loss of BN/UHMWPE composites with different BN content and draw ratio, before and after the thermal annealing treatment. (b–d) The charge–discharge efficiency (η) of drawn pure UHMPWE and BN/UHMWPE composites measured at 100 MV m^{-1}, before and after the thermal annealing treatment.

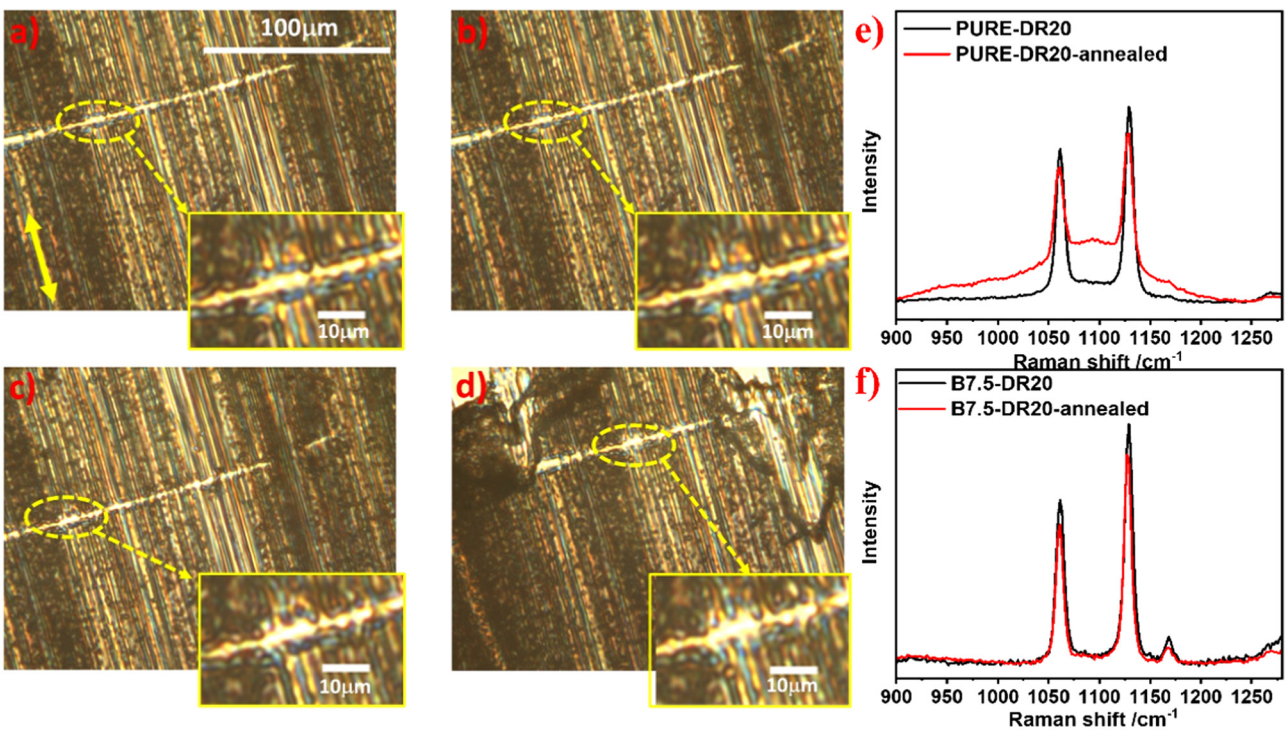

Fig. 7 The *in situ* OPM images of B7.5-DR60 at (a) room temperature, (b) 140 °C, (c) 142 °C and (d) 144 °C. The yellow double arrow denotes the drawing direction. The Raman spectroscopy (between 900 and 1280 cm^{-1}) of (e) PURE-DR20 and (f) B7.5-DR20 before and after anneal treatment at 100 °C for 20 min.

and the η even slightly decreased, suggesting that the anneal treatment did not have any positive healing effect on pure drawn UHMWPE films. Therefore, it is reasonable to speculate that the healing process preferentially happens at/near the filler–matrix interface. Samples with low draw ratio and low filler loading, contain only small longitudinal voids and very few transverse voids, as verified by the OPM (Fig. 1d–l). After the anneal treatment, the positive effect of partially healed longitudinal voids overshadowed the negative effect of enlarged transversal voids, leading to an enhanced breakdown strength and η. However, at increased filler content and/or draw ratio, the negative effect of more transverse voids generated, became the dominant effect, resulting in a largely decreased E_b, *e.g.* for B7.5-DR60.

The observed decrease in thermal conductivity is expected, and ascribed to the reduced chain orientation during anneal treatment, verified by the decreased peak intensity of peaks at 1129 and 1062 cm^{-1} in Fig. 7e and f. To be noticed, these two peaks represent all-*trans* C–C stretching vibrations and thus related to the content of extended chains in both crystalline and amorphous phase (*i.e.* chain alignment).

4. Conclusion

In conclusion, BN was introduced into UHMWPE followed by uniaxially solid-state drawing to fabricate dielectric composite films with high thermal conductivity. The thermal conductivity was increased significantly by BN doping (29% with a 1 wt% BN and draw ratio of 40), but dielectric properties (dielectric loss and breakdowns strength) were sacrificed because of a weak filler–matrix interface and poor filler distribution. A simple thermal annealing treatment was utilised to tackle this problem. After 20 min annealing at 100 °C, the defects located near/at the filler–matrix interface were partially healed, leading to an increase of more than 20% in breakdown strength of composite films with low draw ratios. Compared to the original B1-DR20 film, the annealed film B1-DR20 showed a 20% increase in breakdown strength, up to 421 MV m^{-1}, an increased charge–discharge efficiency of 94% at 100 MV m^{-1} (by 1%). With a high thermal conductivity of 16 W m^{-1} K^{-1}, the annealed film B1-DR20 have great potential in electronic applications such as capacitors, electronic packaging. This finding demonstrates a simple and fast method to tune the dielectric and thermal conduction properties of drawn polymer composites films, without the need of any filler surface functionalisation, which promises widening applicability of polymer films in capacitors, thermal management and substrate technology.

Data availability

The data supporting this article have been included as part of the ESI.†

Conflicts of interest

There are no conflicts to declare.

Acknowledgements

Xiangyan Yu (201906370046) thanks for the research studentship jointly funded by China Scholarship Council (CSC) and Queen Mary University of London. We also thank Zhipeng Lin for his generous help in Transmitted Electron Microscopy (TEM).

References

1 X. Y. Huang, P. K. Jiang and L. Y. Xie, Ferroelectric polymer/silver nanocomposites with high dielectric constant and high thermal conductivity, *Appl. Phys. Lett.*, 2009, **95**(24), 3, DOI: **10.1063/1.3273368**.

2 Y. Li, X. Huang, Z. Hu, P. Jiang, S. Li and T. Tanaka, Large dielectric constant and high thermal conductivity in poly (vinylidene fluoride)/barium titanate/silicon carbide three-phase nanocomposites, *ACS Appl. Mater. Interfaces*, 2011, **3**(11), 4396–4403.

3 D. Cao, W. Y. Zhou, Y. Li, C. Liang, J. Li, D. F. Liu, Y. Wang, T. Li, G. Z. Cao, J. J. Zhou, *et al.*, Tailoring the dielectric properties and thermal conductivity of f-Cu/PVDF composites with SiO_2 shell as an interfacial layer, *Polym.-Plast. Technol. Mater.*, 2022, **61**(4), 400–414, DOI: **10.1080/25740881.2021.1991950**.

4 L. Hu, Y. T. Xia, Q. Q. Wang, H. Yang and Q. L. Zhang, Core-shell structured dendritic CuO@TiO2 for high-k P(VDF-HFP) composites with suppressed dielectric loss and enhanced thermal conductivity, *J. Mater. Sci.: Mater. Electron.*, 2018, **29**(2), 1269–1279, DOI: **10.1007/s10854-017-8032-x**.

5 T. Li, W. Y. Zhou, Y. Li, D. Cao, Y. Wang, G. Z. Cao, X. R. Liu, H. W. Cai and Z. M. Dang, Synergy improvement of dielectric properties and thermal conductivity in PVDF composites with core-shell structured Ni@SiO_2, *J. Mater. Sci.: Mater. Electron.*, 2021, **32**(4), 4076–4089, DOI: **10.1007/s10854-020-05149-x**.

6 W. W. Peng, W. Y. Zhou, G. Z. Cao, Y. T. Yang, J. Cao, F. R. Kong, G. H. Wang, A. H. Feng and L. D. Luo, Towards synchronously improving dielectric performances and thermal conductivity in Ni/PVDF by tailoring core-shell structured Ni@NiO particles, *High Perform. Polym.*, 2022, **34**(10), 1177–1192, DOI: **10.1177/09540083221111320**.

7 H. Y. Wang, Y. B. You, J. W. Zha and Z. M. Dang, Fabrication of BaTiO3@super short MWCNTs core-shell particles reinforced PVDF composite films with improved dielectric properties and high thermal conductivity, *Compos. Sci. Technol.*, 2020, **200**, 8, DOI: **10.1016/j.compscitech.2020.108405**.

8 W. Y. Zhou, Y. J. Kou, M. X. Yuan, B. Li, H. W. Cai, Z. Li, F. X. Chen, X. R. Liu, G. H. Wang, Q. G. Chen, *et al.*, Polymer composites filled with core@double-shell struc-

tured fillers: Effects of multiple shells on dielectric and thermal properties, *Compos. Sci. Technol.*, 2019, **181**, 10, DOI: **10.1016/j.compscitech.2019.107686**.

9 W. Y. Zhou, X. Li, F. Zhang, C. H. Zhang, Z. Li, F. X. Chen, H. W. Cai, X. R. Liu, Q. G. Chen and Z. M. Dang, Concurrently enhanced dielectric properties and thermal conductivity in PVDF composites with core-shell structured beta-SiCw@SiO_2 whiskers, *Composites, Part A*, 2020, **137**, 12, DOI: **10.1016/j.compositesa.2020.106021**.

10 Y. Zhang, F. Zhang, M. Zhang, J. Luo, Y. Shi, R. Yin, G. Wang and W. Zhou, Core-shell engineering of graphite nanosheets reinforced PVDF toward synchronously enhanced dielectric properties and thermal conductivity, *Eur. Polym. J.*, 2024, **215**, 113236, DOI: **10.1016/j.eurpolymj.2024.113236**.

11 X. Chen, Y. Shi, K. Zhang, Y. Feng, J. Zuo, H. Wu, X. Ren and W. Zhou, Synergistically depressed dielectric loss and elevated breakdown strength in core@double-shell structured Cu@CuO@MgO/PVDF nanocomposites, *Polymer*, 2024, **307**, 127321, DOI: **10.1016/j.polymer.2024.127321**.

12 Y. Hattori, T. Taniguchi, K. Watanabe and K. Nagashio, Anisotropic Dielectric Breakdown Strength of Single Crystal Hexagonal Boron Nitride, *ACS Appl. Mater. Interfaces*, 2016, **8**(41), 27877–27884, DOI: **10.1021/acsami.6b06425**.

13 C. J. Wort and R. S. Balmer, Diamond as an electronic material, *Mater. Today*, 2008, **11**(1–2), 22–28.

14 V. Guerra, C. Wan and T. McNally, Thermal conductivity of 2D nano-structured boron nitride (BN) and its composites with polymers, *Prog. Mater. Sci.*, 2019, **100**, 170–186, DOI: **10.1016/j.pmatsci.2018.10.002**.

15 M. Wu, Y. Zhou, H. Zhang and W. Liao, 2D Boron Nitride Nanosheets for Smart Thermal Management and Advanced Dielectrics, *Adv. Mater. Interfaces*, 2022, **9**(25), 2200610, DOI: **10.1002/admi.202200610**(acccessed 2022/11/24).

16 S. Shen, A. Henry, J. Tong, R. Zheng and G. Chen, Polyethylene nanofibres with very high thermal conductivities, *Nat. Nanotechnol.*, 2010, **5**(4), 251–255, DOI: **10.1038/nnano.2010.27**.

17 P. J. Lemstra, N. A. J. M. van Aerle and C. W. M. Bastiaansen, Chain-Extended Polyethylene, *Polym. J.*, 1987, **19**(1), 85–98, DOI: **10.1295/polymj.19.85**.

18 P. Cataldi, P. Steiner, T. Raine, K. Lin, C. Kocabas, R. J. Young, M. Bissett, I. A. Kinloch and D. G. Papageorgiou, Multifunctional Biocomposites Based on Polyhydroxyalkanoate and Graphene/Carbon Nanofiber Hybrids for Electrical and Thermal Applications, *ACS Appl. Polym. Mater.*, 2020, **2**(8), 3525–3534, DOI: **10.1021/acsapm.0c00539**.

19 A. Tomokiyo and T. Okada, Determination of Thermal Diffusivity by the Temperature Wave Method, *Jpn. J. Appl. Phys.*, 1968, **7**(2), 128, DOI: **10.1143/JJAP.7.128**.

20 J. Wu, A. Mahajan, L. Riekehr, H. Zhang, B. Yang, N. Meng, Z. Zhang and H. Yan, Perovskite $Sr_x(Bi_{1-x}Na_{0.97-x}Li_{0.03})_{0.5}TiO_3$ ceramics with polar nano regions for high power energy storage, *Nano Energy*, 2018, **50**, 723–732, DOI: **10.1016/j.nanoen.2018.06.016**.

21 J. Wu, H. Zhang, C.-H. Huang, C.-W. Tseng, N. Meng, V. Koval, Y.-C. Chou, Z. Zhang and H. Yan, Ultrahigh field-induced strain in lead-free ceramics, *Nano Energy*, 2020, **76**, 105037, DOI: **10.1016/j.nanoen.2020.105037**.

22 N. Meng, X. Ren, G. Santagiuliana, L. Ventura, H. Zhang, J. Wu, H. Yan, M. J. Reece and E. Bilotti, Ultrahigh β-phase content poly(vinylidene fluoride) with relaxor-like ferroelectricity for high energy density capacitors, *Nat. Commun.*, 2019, **10**(1), 4535, DOI: **10.1038/s41467-019-12391-3**.

23 X. Ren, N. Meng, H. Zhang, J. Wu, I. Abrahams, H. Yan, E. Bilotti and M. J. Reece, Giant energy storage density in PVDF with internal stress engineered polar nanostructures, *Nano Energy*, 2020, **72**, 104662, DOI: **10.1016/j.nanoen.2020.104662**.

24 R. V. Gorbachev, I. Riaz, R. R. Nair, R. Jalil, L. Britnell, B. D. Belle, E. W. Hill, K. S. Novoselov, K. Watanabe, T. Taniguchi, *et al.*, Hunting for Monolayer Boron Nitride: Optical and Raman Signatures, *Small*, 2011, **7**(4), 465–468, DOI: **10.1002/smll.201001628**(acccessed 2023/05/24).

25 D. Golberg, Y. Bando, Y. Huang, T. Terao, M. Mitome, C. Tang and C. Zhi, Boron Nitride Nanotubes and Nanosheets, *ACS Nano*, 2010, **4**(6), 2979–2993, DOI: **10.1021/nn1006495**.

26 G. R. Strobl and W. Hagedorn, Raman spectroscopic method for determining the crystallinity of polyethylene, *J. Polym. Sci., Polym. Phys. Ed.*, 1978, **16**(7), 1181–1193, DOI: **10.1002/pol.1978.180160704**(acccessed 2023/06/11).

27 M. Pigeon, R. E. Prud'homme and M. Pezolet, Characterization of molecular orientation in polyethylene by Raman spectroscopy, *Macromolecules*, 1991, **24**(20), 5687–5694, DOI: **10.1021/ma00020a032**.

28 Y. Men, J. Rieger, H.-F. Endeler and D. Lilge, Mechanical α-Process in Polyethylene, *Macromolecules*, 2003, **36**(13), 4689–4691, DOI: **10.1021/ma0344902**.